GEOPHYSICS, VOL. 77, NO. 5 (SEPTEMBER-OCTOBER 2012); P. WC47–WC58, 17 FIGS., 2 TABLES.
10.1190/GEO2011-0487.1

3D seismic imaging of volcanogenic massive sulfide deposits in the Flin Flon mining camp, Canada: Part 1 — Seismic results

D. J. White[1], D. Secord[2], and M. Malinowski[3]

ABSTRACT

A 17-km^2 3D-3C seismic survey was conducted within the active Flin Flon mining camp located in Manitoba, Canada. The results for the vertical component data as obtained by conventional dip-moveout and prestack time-migration processing sequences and comparison of images from the 3D seismic volume with the subsurface location of known ore zones and the mine horizon generally showed a very good correlation. A well-defined diffraction response from the shallowest ore zone was observed in the unmigrated data with a corresponding phase reversal in the migrated data at the transition from intact ore to backfilled ore zone. The geometry of unmined and backfilled ore zones compared well with strong reflection amplitudes on corresponding cross sections to depths of ~1000 m. At greater depths, the ore zone had a weaker seismic signature due to a combination of effects, including imaging conditions, ore composition, and the increased presence of rhyolite within the mine horizon. In the case of the deeper ore zones that were characterized by low signal-to-noise levels, poststack migration was important in focusing weak ore-related reflections. The 3D data demonstrated the feasibility of detecting and accurately locating ore zones as small as a few million tons to depths of up to 1500 m.

INTRODUCTION

The Flin Flon mining camp in Manitoba, Canada, forms part of the largest Paleoproterozoic volcanogenic massive sulfide (VMS) district in the world, hosting 24 deposits with aggregate tonnage of 143 Mt of sulfide in past or producing mines and an additional 64 Mt contained in subeconomic or preproduction deposits (Galley et al., 2007). Regional exploration within the Flin Flon area has historically been dominated by the use of airborne, ground-based, and drillhole electromagnetic and magnetic surveys with greater than 60% of the discoveries in the camp having been credited to geophysical methods (Jones, 2001). In 2007, a 17-km^2 3D-3C seismic survey was conducted within the Flin Flon mining camp in an attempt to explore to greater depths than are attainable using conventional electromagnetic techniques (e.g., Eaton et al., 2010). Specific objectives included: (1) mapping the mine horizon at depth including offsetting fault zones, (2) testing the ability to directly image the known ore deposits, and (3) establishing new exploration drill targets. In this paper, we focus on the acquisition and processing of the vertical component seismic data with the intent of providing a reference for further application of 3D seismic surveys in hard-rock environments. We then address the ability to image the known ore deposits within the camp. A complementary companion paper (Malinowski et al., 2012) describes the results of seismic modeling of a 3D model for the camp.

GEOLOGY AND ORE DEPOSITS OF THE FLIN FLON CAMP

The Flin Flon mining camp (Figure 1) lies within the Paleoproterozoic Flin Flon metavolcanic belt, which consists of polydeformed supracrustal and intrusive rocks (Syme and Bailes, 1993). The volcanic rocks of the Flin Flon arc assemblage are unconformably overlain by continental alluvial sediments (arkoses, greywacke, conglomerate, and argillite; referred to hereafter as "Missi sandstones") and intercalated volcanic rocks of the Missi Group. The main sulfide deposits of the Flin Flon camp comprise predominantly pyrite, pyrrhotite, sphalerite, and chalcopyrite. The Flin Flon Main, 777, and Callinan deposits occur in the west limb of the Hidden Lake synform residing within a 200-m-thick package of rhyolitic flows and breccias (mine rhyolite of the Millrock member)

Manuscript received by the Editor 30 November 2011; revised manuscript received 23 March 2012; published online 6 September 2012.
[1]Geological Survey of Canada, Ottawa, Ontario, Canada. E-mail: don.white@nrcan.gc.ca.
[2]Sensor Geophysical Ltd., Calgary, Alberta, Canada. E-mail: djsecord@shaw.ca.
[3]Polish Academy of Sciences, Institute of Geophysics, Warsaw, Poland. E-mail: michalm@igf.edu.pl.

that is sandwiched between basalt-dominated rocks of the stratigraphic footwall and the hanging wall. The volcanic basement rocks are in thrust contact with the younger Missi Group sandstones along the Club Lake fault. Other interpreted thrust faults at the north end of the Hidden Lake synform (Figure 1) suggest that the ore-bearing horizon may be replicated at depth. The massive 62.4 Mt Flin Flon Main deposit, which was discovered in 1915, ceased production in 1990. Production of several smaller deposits in the area (e.g., 777 [14.2 Mt] and Callinan [8.4 Mt]) continues to supply the smelter in Flin Flon.

The Callinan and 777 ore deposits lie within the area covered by the 3D seismic survey. At the time of the seismic survey in 2007, the Callinan ore deposits were mostly depleted, whereas the 777 ore lenses were largely still intact. Mined-out zones are backfilled with crushed waste rock in either an unconsolidated or a "cemented" form. The Callinan ore deposit was originally composed of a series of discrete lenses arranged in an *en echelon* pattern extending from 250 to 1150-m depth. The bulk of the deposit was constituted by several large lenses that are typically elongate (600–1000 m in extent), narrow (50–200 m wide), and generally thin (less than

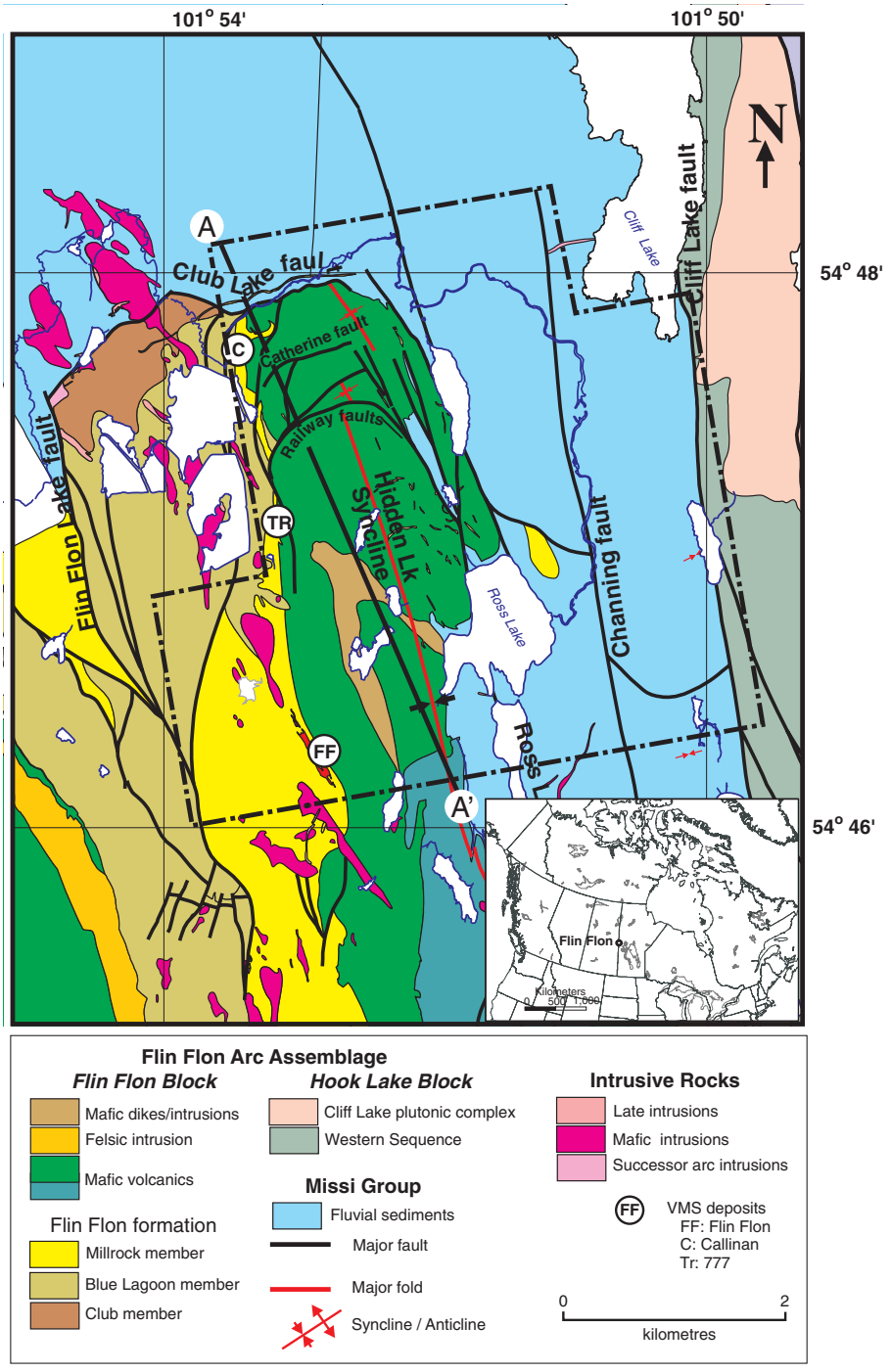

Figure 1. Geology map showing area of 3D seismic survey. Inset shows the location of Flin Flon. Approximate locations of the VMS deposits (C, TR, FF) are shown near the location where the hosting unit (Millrock member) outcrops at the surface. The actual location of the individual ore lenses is shown in detail in Figure 3.

10 m ranging up to 30 m thick). They have moderate dips (40° to 52°) with dip azimuths of 96° to 105° east of north. The deeper 777 deposit similarly is composed of several narrow lenses that are up to 1000 m in length and are generally less than 20 m thick. The 777 lenses compositely extend from 900 to 1600-m depth. They have similar dips (39° to 44°) to the Callinan ore lenses, but the dip azimuths (120° to 125° east of north) are more southerly. Generally, the 777 ores are more massive than the Callinan ore that tends to be more typically brecciated. Also, the 777 ores and Callinan ores are pyrrhotite- and pyrite-rich, respectively.

THREE-DIMENSIONAL REFLECTION SEISMICS FOR MINERAL EXPLORATION

Three-dimensional seismic surveys for the purposes of mineral exploration have been conducted at a variety of locations in Canada (e.g., Sudbury, Milkereit et al., 1997; Matagami, Adam et al., 1997; Bathurst, Gingerich et al., 2002; Malehmir and Bellefleur, 2009; Louvicourt mine, Adam et al., 2007; see Eaton et al., 2010 for a summary), South Africa (e.g.,Vaal Reefs Gold Mine, Pretorius et al., 1997), Finland (Kevitsa; A. Malehmir, personal communication, 2012), and Australia (Oxiana, Kanowna, Kambalda, Cannington, Century, and Ranger; M. Urosevic, personal communication, 2011.). The first documented case of an exploration success where 3D seismic imaging was used for VMS exploration occurred at the Bathurst camp in Canada (Gingerich et al., 2002).

Over the past 10 years, there have been significant advances in seismic recording systems that make these systems better suited for mineral exploration in complex geologic environments and across shield-type terrains. The number of recording channels has increased so that more than 10,000 channels are commonly available. This provides opportunity for more complete spatial sampling, recording of longer offset data, and the capacity to record multicomponent data. Wireless acquisition systems make field deployments less cumbersome and significantly more flexible for aiding deployments in difficult terrain. Single-sensor recording largely eliminates the dip-filtering effects inherent in recording with sensor arrays as well as reducing the amount of equipment to be deployed. Three-component sensors encased within a single housing make the deployment effort comparable to conventional single-component sensors affording the ability to acquire multicomponent data. These technological advances were exploited during 3D seismic acquisition in the Flin Flon camp in 2007 where a 3D survey for VMS exploration was conducted for the first time using 3C sensors and with ~9000 live channels. Previous seismic work in this area consisted of a pioneering exploration test conducted by Hajnal and Stauffer (1975) and regional seismic data acquisition during the LITHOPROBE project (e.g., Lucas et al., 1994; White et al., 1994).

THE FLIN FLON 3D SEISMIC SURVEY

Presurvey assessments and survey design

Seismic properties of rocks from the Flin Flon VMS camp were determined to evaluate the suitability of seismic reflection imaging for mineral exploration prior to conducting seismic acquisition. Seismic properties were determined at a variety of scales including laboratory measurements on core samples, in situ logging measurements of V_P and density, and acquisition of vertical seismic profiles. The seismic impedances summarized in Figure 2 illustrate that Missi sandstones and rhyolites will have mean reflection coefficients of up to $R = 0.08$ relative to the predominantly basaltic country rock, and the mean reflection coefficients of the ore zones, though variable, will generally be higher ($R = 0.08$ to 0.30). Thus, the mine horizon that is characterized by the presence of rhyolite and ore zones (locally) should generally be reflective although significant variability is expected due to alteration of the footwall basalt. The seismic properties of the backfill material have not been measured, but the acoustic impedance should be relatively low as the backfill consists of crushed country rock in unconsolidated form or mixed with a cohesive. As a proxy for the backfill material, we consider the broad range of impedances of porous sandstones (see Figure 2), reflection coefficients of at least 0.15 would be expected. Thus, the mined-out zones should have comparable geometry to the original ore deposits with strong reflectivity, but the reflections should have opposite polarity.

The area to be covered in the 3D seismic survey was chosen to cover key features of the geology within the camp. Of particular interest was determination of (1) the extent of the volcanic host units eastward beneath the Missi sandstones, and (2) the potential existence of thrust repetitions of the mine horizon in the vicinity of

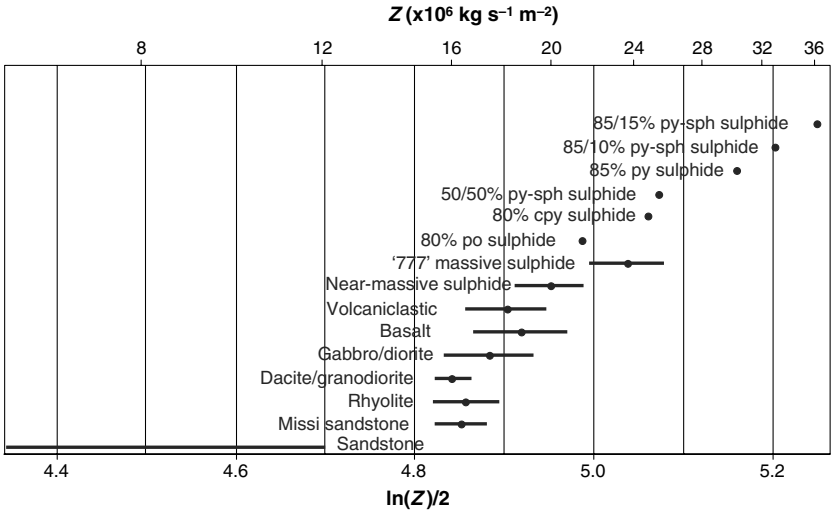

Figure 2. Mean acoustic impedance (Z) versus lithology is shown (top axis) and $\ln(Z)/2$ is displayed on the lower axis. The mean normal-incidence reflection coefficient (R) for any two lithologic units is obtained by taking the difference in values from the lower axis (i.e., $R \approx \Delta(\ln Z)/2$; Sheriff and Geldart, 1984, p. 76). The values shown with error bars are mean values (±1 standard deviation) as determined from downhole sonic logs, and the single points represent measurements made on core samples. Log-based mean values were determined from hundreds of individual measurements for each rock type with the exception of the sulfides where there were only 40 measurements in total. The range of values for "sandstone" is from Sheriff and Geldart (1984), p. 119.

the existing mines. With these goals in mind, and subject to budgetary restrictions, the 3D area was extended from the surface trace of the mine horizon in the west (Millrock member in Figure 1) to the eastern boundary of the Missi sandstones, and from the northern limit of the Flin Flon volcanics (Club Lake fault in Figure 1) to south of the existing 777 ore deposits. The depth interval of interest was approximately 500–3000 m. Regional structure information was accounted for during the design of the 3D survey to ensure adequate coverage of the zone of interest. Specifically, the expected reflection/scattering of seismic energy in the down-dip direction was modeled using simple ray-tracing methods to determine how large the surface deployment of sensors would have be to achieve adequate imaging. Over the depth interval of interest (500–3000 m) within the central part of the survey area, ray-tracing results indicate that the maximum detectable dips will decrease from ~75° at 500-m depth to ~30° at 3000-m depth.

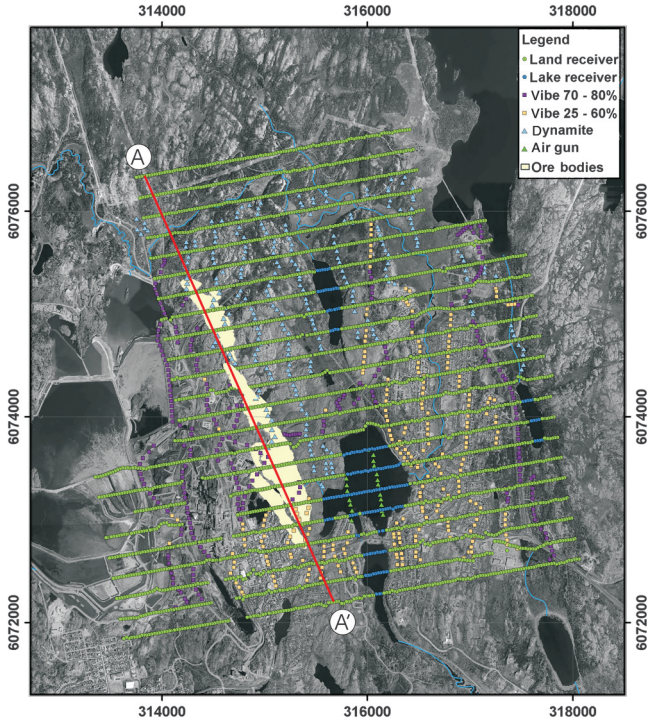

Figure 3. Airphoto with 3D survey geophone and source positions. Also shown are the ore zone locations vertically projected to the surface, and the line of section A-A′ from Figure 1. The *y*- and *x*-axes are annotated with northings and eastings (in meters), respectively.

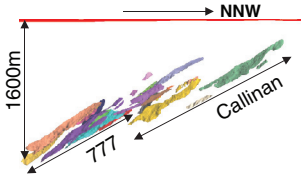

Figure 4. Vertical section perspective view of the Callinan and 777 ore lenses. View is from the east-northeast approximately orthogonal to the profile A-A′ shown in Figure 1.

Data acquisition

The Flin Flon mining camp presents a challenging environment for geophysical exploration. The community of Flin Flon is an active mining town with a population of approximately 7000. It has developed over the years around the original open pit mine and sits immediately above the ore deposits that are currently being mined (see Figures 3 and 4). The area of interest for the 3D seismic survey encompasses a variety of land uses (Figure 3), including parts of the mine operations (mill, smelter, and tailings ponds), central business section (paved roads and small office buildings), and residential areas. This setting makes for difficult acquisition logistics presenting a relatively noisy background for seismic recording and limiting the strength of seismic sources that could be employed. The natural terrain within the 3D area also is highly variable comprising exposed bedrock, swamps, pockets of shallow glacial deposits, and lakes.

The survey area covered ~17 km^2, including 940 shotpoints and 3378 receiver stations. A conventional regular orthogonal grid of shot and receiver lines was adopted with nominal station locations subsequently adjusted according to site accessibility. As can be seen in Figure 3, only minor modifications were required for receiver stations/lines, whereas the shot station locations were largely controlled by the network of roads. Receiver lines were oriented approximately east–west to provide finer spatial sampling in the direction of predominant regional dip. Operations from the start of shot-hole drilling to the completion of data acquisition occurred from 19 June to 5 September 2007. The number of live stations per shot ranged from 2670 to 2890 (or 8010 to 8670 channels), for a total of 2.75 million data traces for the survey. Table 1 provides details of the acquisition parameters.

Energy sources used in the survey were vibroseis, dynamite, and air guns (see Figure 3 and Table 1). Vibroseis was used wherever there was access by road or trail. Vibroseis peak force was reduced from the standard operation level of 80% to 25% in residential and downtown areas. As a result, ~50% of the vibroseis shotpoints were acquired with reduced energy levels. Dynamite shots were deployed in two different manners. The preferred deployment method based on presurvey vertical seismic profile (VSP) tests utilized a single drillhole penetrating 5 m into bedrock and loaded with 0.5 kg of dynamite. This was implemented for shotpoints that were accessible either using small tracked air drill units or heli-portable drills. At each of the remaining dynamite shotpoints, 0.1 kg of dynamite was loaded into each of three 1–1.5-m-deep drillholes drilled into exposed bedrock with a gas-powered hand drill. In Ross Lake, a small airgun charged with compressed nitrogen was used with four air-gun pops fired at each of 23 shotpoints. Due to timing issues with the air gun trigger, these data were not used in the final processing flow.

Several modes of geophone deployment were required to adapt to the local terrain (see Table 1 for a summary). For exposed bedrock sites, sensors were placed in shallow drillholes with the horizontal components oriented with a compass. Where unconsolidated surface material was available, the sensors were buried. Sensors were deployed in Ross Lake at depths less than 20 m using sand bags to ensure coupling on the lake bottom with cabling running to recording units positioned in inflatable boats. The Vectorseis 3C sensors used in the survey are accelerometers that are capable of operating at any deployment angle. They also use the local gravitational field to determine the tilt of the individual components, which can be

used to correct for tilt in the vertical component. In the business section of town, sensors were deployed on the pavement in sand-filled buckets.

Data processing

Overall, the data quality ranged from poor to good as would be expected given the high level of cultural noise in the area. Mean signal-to-noise estimates show a strong correlation with land-use in the area with generally lower signal-to-noise levels in the central and south-central regions of the survey. Examples of shot gathers for dynamite and vibroseis sources are shown in Figure 5. Clear first breaks are observed (Figure 5a and b) to offsets of greater than 3000 m. The most prominent features observed on the gathers are the direct refraction arrivals (P-wave and S-wave) and ground roll, with the direct S-wave arrival and ground roll being somewhat stronger on the vibroseis record. Reflection/diffraction energy is clearly much weaker, although some weak reflections can be identified under close scrutiny of the records. The power spectra for both source types vary by less than 6 dB over the vibroseis sweep frequency range (30–160 Hz), but the dynamite spectrum is broader (5–180 Hz). Vibroseis stack traces were match-filtered to dynamite stack traces with bulk shift and phase rotation values determined by match-filtering separate stacks of vibroseis or dynamite data within the time window of 2.5–3.5 s. Vibroseis polarity appeared to be opposite to the dynamite polarity.

An overview of the processing flow and associated parameters are provided in Table 2. Standard common depth point (CDP) bin dimensions of one-half the inline shot spacing and one-half the inline receiver spacing were adopted resulting in bin dimensions of 25×12.5 m (north–south, east–west). The resultant stack fold was as high as 200 in the center of the survey but reaching at least 40 over most of the area (Figure 6a). To obtain a measure of the fold that accounts for the variable source energy over the survey area, the stack fold shown in Figure 6b has been adjusted for cumulative source effort. This was done by applying source weighting factors for each source-receiver pair in the fold calculation. Dynamite shots were assigned a weight of one and vibroseis sources were scaled according to the corresponding peak force (scale factors of 0.25 to 0.8; see Figure 3). As can be seen in Figure 6b, the maximum fold is reduced to ~150 and is significantly reduced in the southern part of the survey area. Noisy traces were eliminated during trace editing, which resulted in ~9% total data loss and up to 15% of the total traces for some individual shot records that were affected by sporadic noise pulses of unknown origin.

Significant effort was devoted to optimization of static corrections, which often is the most important step in obtaining good imaging results in crystalline terranes (e.g., Milkereit et al., 1994; Adam et al., 2003; Roberts et al., 2003). In addition to applying refraction and residual statics, manual statics were determined by applying linear moveout to "flatten" the first break trajectories, and then visually inspecting the first breaks for trace-to-trace offsets or unusual traveltime deviations. However, the stack obtained using only refraction and residual statics proved to be adequate and thus only these statics were adopted for final processing. Combined refraction and residual statics were generally in the range of ±10 ms for shots and receivers, respectively. Examples of processed shot gathers are shown in Figure 7, where an observable reflection (R) has been noted.

A conventional dip-moveout (DMO) time processing flow was implemented with significant effort invested in velocity analysis. As is common with data characterized by generally weak, discontinuous

Table 1. Seismic acquisition and CMP parameters.

Source parameters	
Total number of source points	940
Source types	Vibroseis, dynamite, air gun
Shot interval and line spacing	50 m, 200 m (variable)
Shot line orientation	NNW
Number of shot lines	14
Dynamite shots	314 shots; 282 with 0.5 kg at 5 m depth and 32 with three 0.09 kg in separate 1.5-m-deep drillholes
Vibroseis	603 shotpoints; 302/301 25%/80% peak force
Configuration	2 × 24,000 kg IVI Y-2400 (Mark-IV) Vibes "nose-to-tail"
Sweeps	Five 15 s sweeps, 30–160 Hz nonlinear with 3 dB per octave boost
Airgun	23 shotpoints, four pops/shotpoint, 2000 psi
Recording parameters	
Total number of receiver stations	3378 (including dead stations)
Receiver type	Single I/O Vectorseis SVSM 3C sensor at each receiver station
Receiver azimuth	240°
Receiver interval and line spacing	25 and 200 m
Receiver line orientation	WSW
Number of receiver lines	23
Typical recording patch	19 lines × 152 stations (3600 × 3775 m)
Maximum live channels	2888
Antialias filter	3/4 Nyquist minimum phase
Notch filter	Out
Sample interval	2 ms
Record length (correlated)	4.0–4.5 s
Survey area	16.4 km^2
CMP bin parameters	
Bin size	25 m(north-northwest) × 12.5 m(west-southwest)
Inlines (north-northwest)	1–171
Crosslines (west-southwest)	1–345
Number of bins	58,995

reflections, velocity spectra were ineffective in assessing appropriate stacking velocities; thus, constant velocity stacks were used to evaluate velocities. Velocities ranging from 5640 to 6480 m/s were investigated during velocity analysis and DMO based on VSP velocity data that suggested a limited range of in situ velocities in the neighborhood of 6000 m/s (see Figure 8). Geologic contacts constrained by drillhole logs were used to make qualitative assessments of the stack results for varying velocities. A constant velocity of 6000 m/s was adopted for NMO/DMO as it produced results that appeared to be as good as spatially varying velocity models. A velocity of 5400 m/s (90% stacking velocity) was used for poststack time migration. Prior to migration, the 3D data volume was interpolated to produce 12.5-m-equidimensional CDP bins.

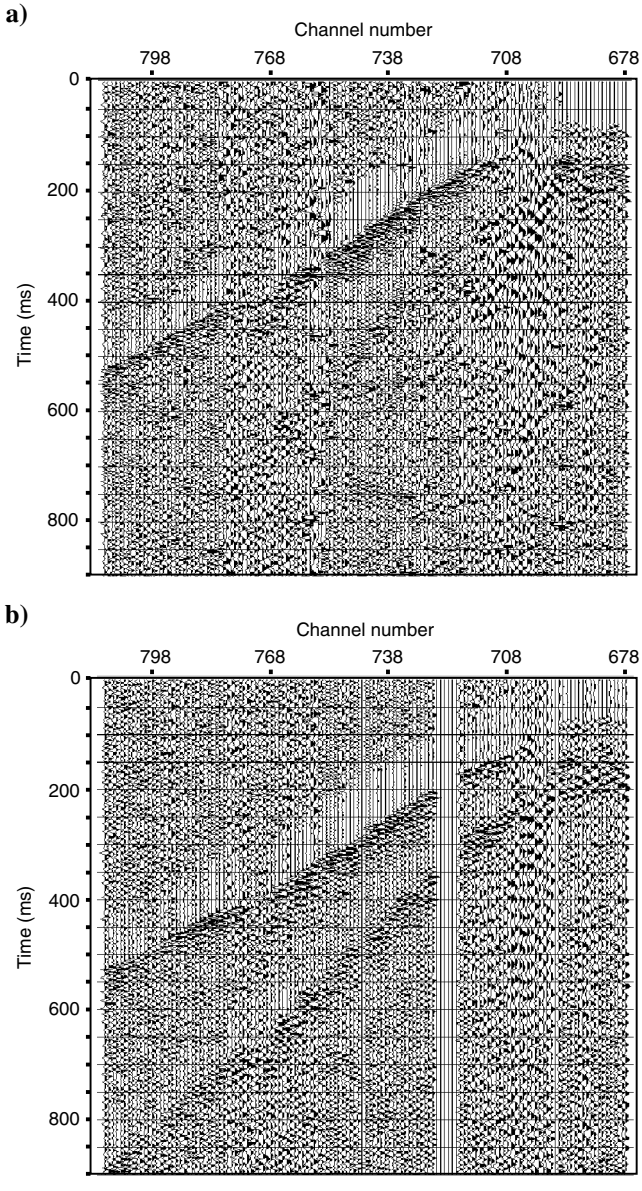

Figure 5. Comparison of raw shot gathers for (a) dynamite and (b) vibroseis shot records recorded along receiver line 113. The two shotpoints are very close. For display, the data have been band-pass filtered 25/30–160/180 and scaled with a 200-ms AGC.

Prestack time migration (PSTM) was attempted in recognition of the potential impact that structural complexity may have on conventional stack (or DMO) imaging. Velocities ranging from 94% to 112% of 6000 m/s with 2% increments were used for prestack migration velocity analysis. Constant velocity stacks were produced and visually compared in a manner similar to the poststack processing results. A final constant velocity model of 6000 m/s was chosen because it produced results that appeared to be at least as good as the 3D variable velocity model constructed based on the individual constant velocity migration stacks. Finally, comparison of the poststack migration, poststack DMO migration, and PSTM volumes indicated that the DMO migration version generally produced the best results. This subjective assessment was done by comparing the volumes with subsurface geology known from drillhole data. The PSTM results were generally poor (see Figure 9 for a comparison). We speculate that this may be due to the low signal-to-noise ratio of the prestack data and the greater sensitivity of PSTM to errors in the migration velocities. Malinowski et al. (2012) show that in the absence of noise and with accurate velocities, pre- and poststack time migration processing flows produce comparable results for synthetic seismic data generated for the complete 3D survey. Other possible contributing factors may include the use of statics determined on CDP gathers rather than on common reflection point (CRP) gathers (although the combined refraction/residual statics are relatively small; ±10 ms) or the lower fold of the common offset vector bins used in PSTM as compared with the common offset bins used in DMO. Further work is required to provide a definitive assessment of the disparity in pre- and poststack migration results.

RESULTS

A vertical slice through the final 3D seismic volume is shown in Figure 10. This section (profile A′-A in Figures 1 and 3 for location) contains the regional plunge of the Hidden Lake synform and directly overlies the Callinan and 777 ore deposits. A prominent zone of semicontinuous reflectivity ("T" indicated by arrows in Figure 10) dips from the near-surface at the north-northwest end of the section to a depth of ~1250 m. Comparison of this reflective zone with the subsurface location of the ore lenses and mine horizon generally shows a very good correlation suggesting that the ore zones are the primary source of these reflections. Also noted on the section in Figure 10 is a prominent reflection (T1) located near 1200 m depth at the north-northwest end of the line that corresponds to a contact between the Missi sandstones and an underlying gabbro body as determined in an exploration drillhole.

The interpreted association of the reflective zone T (in Figure 10) with the ore zones is corroborated in Figure 11, which shows a strong unmigrated diffraction response (labeled "D"') from the shallowest Callinan ore lens identified by its characteristic semicircular shape and strong amplitudes in the down-dip direction. This response can be followed to depth in unmigrated depth slices (Figure 12). Direct comparison of the Callinan ore lenses with vertical slices through the migrated volume (Figure 13) also show a strong correspondence between the ore bodies and the geometry and amplitude of reflections. Note that a phase reversal is observed in Figure 13a. This interpreted phase reversal also is observed on an orthogonal slice (Figure 14) and corresponds approximately to the depth where there is a transition from intact ore above, to the backfilled ore zone below. As discussed earlier, a phase reversal would be expected where a high-impedance

ore zone changes laterally to a low-impedance backfill zone. This abrupt lateral change in the phase of the reflection could alternatively be interpreted as a subvertical fault offset, but the ore zone is mapped continuously through this zone.

In contrast to the clear definition of the Callinan ore zone in the seismic images, the deeper 777 deposit appears to have a much weaker response as shown in Figure 10. There is little indication of a significant diffraction response when compared with that

Table 2. Seismic processing sequence.

Processing	Parameters
1. First-stage processing flow	
Assign geometry	
Extract vertical component data	
Correlate vibroseis records	
Mean fold	47
Number of traces	2,748,434
Trace edits	(114,438 dead, 137,337 killed)
Bulk shift airgun records	450 ms
Sinusoidal noise removal	60, 120 Hz
Spherical divergence correction, gain	$1/tv^2$, 6 dB/s
Attenuate air blast	
Surface-consistent spiking deconvolution	One window, 100 ms operator, 0.1% white noise
Deconvolution compensation to vibroseis records	−8.5 ms time shift and −170° phase rotation
Time-variant spectral whitening	Frequency band 10/20–160/170, 14 frequency panels; scalar length 200 ms
Pick first arrival traveltimes	0–1500-m offset
Refraction statics (Hampson-Russell GLI3D)	One layer, 350 m datum, replacement velocity 6000 m/s
Velocity analysis	Constant velocity stacks (5640–6480 m/s)
Residual statics (power autostatics); three passes	0.3–3.3 s, maximum shift = ± 15 ms
2a. Stack/poststack time migration flow	
DMO	6000 m/s
NMO	6000 m/s
Top mute	50 m:0 ms, 240 m:47 ms, 1350 m:155 ms
Automatic gain control (AGC)	200 ms window
CDP stack	Mean
f-xy deconvolution	3 inlines × 6 crosslines; 100 ms window; overlap 50 ms; 10–170 Hz
Trace interpolation	To 12.5 m × 12.5 m bins
Phase-shift migration	Up to 90° dips; V = 6000 m/s; 5–170 Hz
Band-pass filter	20/30–80/90 Hz zero-phase Ormsby
Trace equalization	Mean, 400–3400 ms
2b. Prestack time migration/stack flow	
(Option) Common offset vector binning	IL offset bin centers −3300–2700 m, inc = 1200 m XL offset bin centers −2750–2750 m, inc = 500 m
f-xy deconvolution	3 inlines × 6 crosslines; 100 ms window; overlap 50 ms; 10–170 Hz
Inverse normal moveout correction	V = 6000 m/s
Prestack time migration velocity analysis	Selected E-W inlines separated by 200 m; 5640–6480 m/s; increments = 120 m/s
Kirchhoff prestack time migration	Maximum dip 65°; V = 6000 m/s
Top mute	50 m:0 ms, 240 m:47 ms, 1350 m:155 ms
AGC	200 ms window
Stack	Mean
Band-pass filter	20/30–80/90 Hz zero-phase Ormsby
Trace equalization	Mean, 400–3400 ms

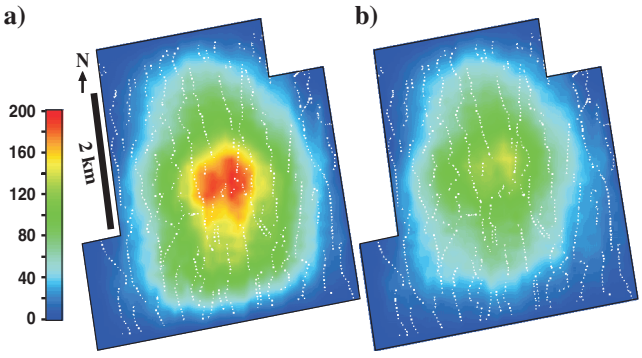

Figure 6. Data fold. (a) Stack fold. (b) Stack fold adjusted by cumulative source effort. See main text for details. In that the air-gun shots in Ross Lake were not used in the final processing flow, they have not been accounted for in the cumulative source effort calculation.

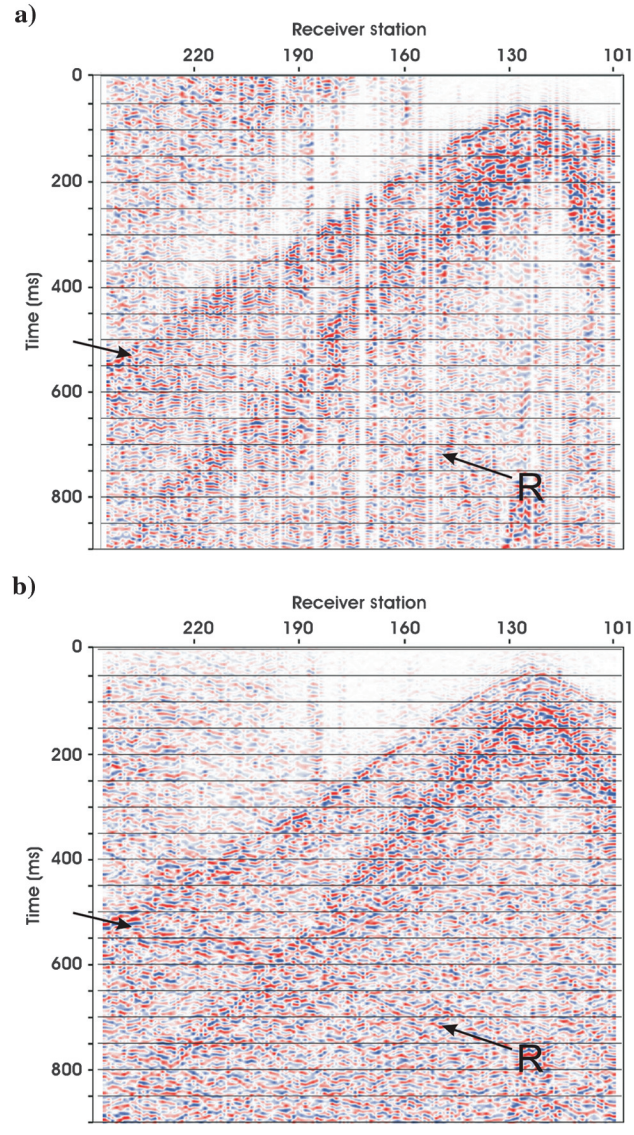

Figure 7. (a) Unprocessed shot gather and (b) same processed to prestack (excluding mutes, DMO, and NMO). Label "R" indicates a reflection.

observed in the case of the Callinan deposit. Inspection of vertical slices through the migrated seismic cube show a generally weak correlation of the reflector geometry and amplitude with the 777 lenses (Figure 15). Factors that likely contribute to this observed variability in the seismic response include imaging conditions, ore composition, and host lithology. Each of these is considered below with reference to the companion modeling paper by Malinowski et al. (2012).

DISCUSSION

Imaging conditions

Generally, the ore lenses constitute thin layers relative to the predominant seismic wavelength of the data and have limited lateral extent as compared with the Fresnel zone. Thus, the observed reflection amplitudes will generally be less than expected from those predicted from rock property measurements (see Figure 2) and they will be subject to tuning effects. The associated wavelengths (λ) are within the range of 120–70 m for peak frequencies of 50–90 Hz, respectively, implying that the individual ore lens thicknesses lie within the range of $\sim 1/2$ to 1/20 of a wavelength. Considering the relatively low signal-to-noise ratio of the 3D data, and the dependence of thin layer detection limits on signal-to-noise ratio, we optimistically consider that minimum thicknesses of 9–15 m (i.e., $\lambda/8$) are likely detectable. Based on this criterion alone, the main ore zones from the Callinan and 777 deposits should produce observable reflections given their comparable thicknesses (10–30 m). However, the fractional area of the first Fresnel zone constituted

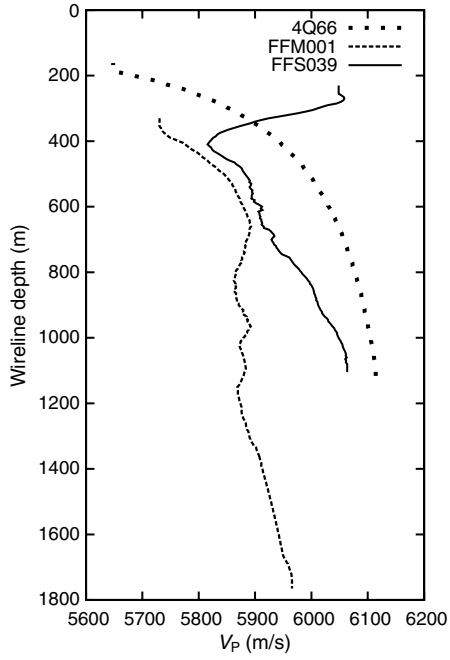

Figure 8. Average velocity versus depth determined from first break picks made on near-offset VSP data from three drillholes in the camp. The velocity curve characterized by consistently lower velocities (~5900 m/s) is for drillhole FFM001 that predominantly penetrates Missi sandstones. Drillhole locations are shown in Figure 1.

by the ore lenses decreases from a maximum of ~0.8 at 500 m depth to ~0.4 at 1500 m depth due to the corresponding increase in Fresnel zone size with depth. This would result in a corresponding decrease of ~50% in the ore zone reflection amplitude for the deepest 777 ore zones relative to the shallow Callinan ore zones. The 3D survey geometry and noise characteristics also may contribute to the weaker reflections from the 777 deposit. The southernmost 777 ore lens lies ~500 m from the edge of the 3D cube where the migration aperture for a structural dip of 45° is ~1060 m. Also, the effective stack fold (Figure 6) decreases toward the southern part of the survey area.

As noted, the deeper ore zones do not show a prominent reflection/diffraction response in the unmigrated data. However, in the migrated data volume the reflections from the deeper ore zones, though weaker, are observable above the background noise (see Figure 16) presumably due to the focusing effects of poststack migration. This suggests that in low signal-to-noise environments, the migrated data may be more effective for direct ore detection, in contrast to higher signal-to-noise cases in which the characteristic directional diffraction response can be observed in the unmigrated data (e.g., Milkereit et al., 1997; Adam et al., 2003; Malehmir and Bellefleur, 2009). Modeling to test the effects of signal-to-noise on the migration process by Malinowski et al. (2012) demonstrate this effect.

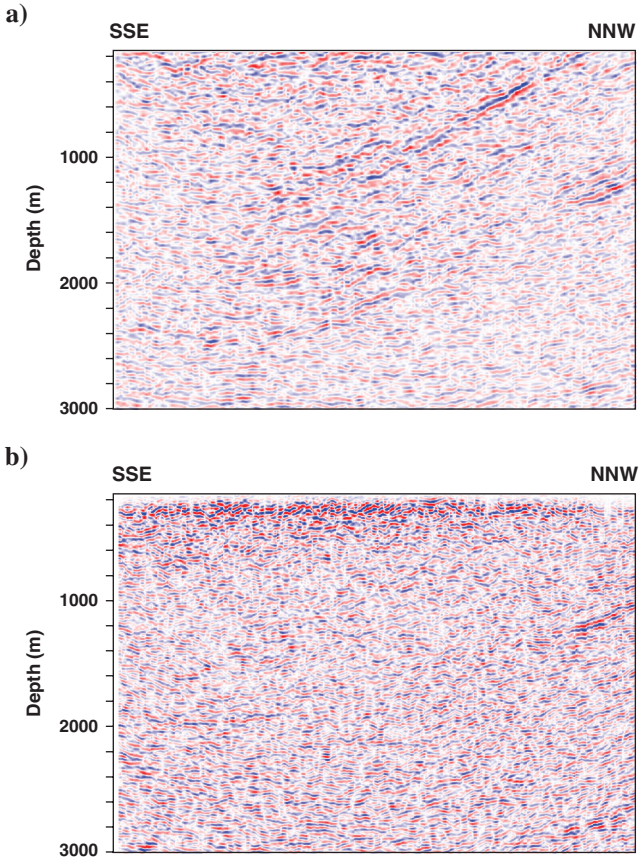

Figure 9. Comparison of final migrated stack for (a) poststack migration and (b) prestack time migration. A constant velocity of 6000 m/s was used for migration in both cases. Vertical slice is taken along a plunge-parallel azimuth. A 20/30–80/90 Hz bandpass filter has been applied for display purposes. Horizontal scale = vertical scale.

Ore composition

The acoustic impedances of sulfide ores are strongly affected by the abundance of the Fe-bearing minerals pyrite and pyrrhotite (see Figure 2). The 777 ores are commonly massive and pyrrhotite-

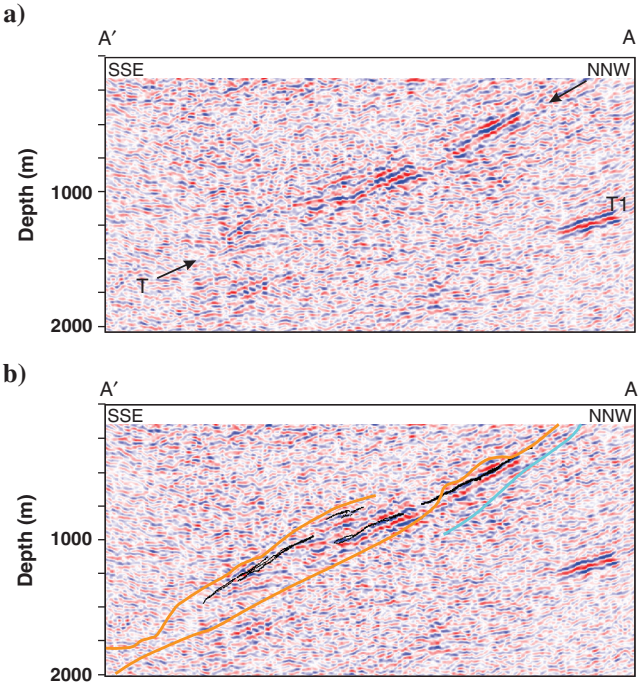

Figure 10. Vertical slice through the migrated 3D seismic volume along section A-A′ (see Figures 1 and 3 for location). (a) Seismic data, and (b) seismic data with drillhole defined geological surfaces; black = ore zones, orange = upper surfaces of Millrock Member, cyan = Club Lake fault. The orientation of the section is approximately aligned with the plunge of the ore zones. The labeled features (T and T1) are referred to in the main text. Horizontal scale = vertical scale.

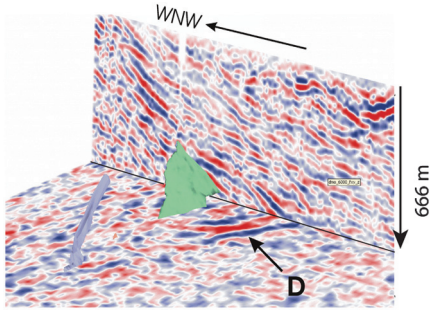

Figure 11. Horizontal slice at 666 m depth and west–east vertical slice from the unmigrated DMO stack volume with Callinan ore lenses shown (in green and purple). Label "D" points to a diffraction from the ore zone.

dominant, which would place their expected acoustic impedances toward the lower end of those shown for sulfide ores, and thus, potentially result in lower amplitude reflections relative to the Callinan ore zone, as observed. Malinowski et al. (2012) show that the strong diffraction response of the 777 ore zone is substantially reduced relative to the background reflectivity for the case of pyrrhotite ore as compared with mixed ore. In contrast, the original Callinan ores were typically pyrite-dominant, suggesting they would be very reflective. The backfilled Callinan ore zones also would be expected to be very reflective due to the low acoustic impedances expected for the fill material, although these reflections would have opposite polarity to ore reflections. This is consistent with the strong reflections observed for the Callinan ore zones and the identified phase-reversal (Figures 13a and 14).

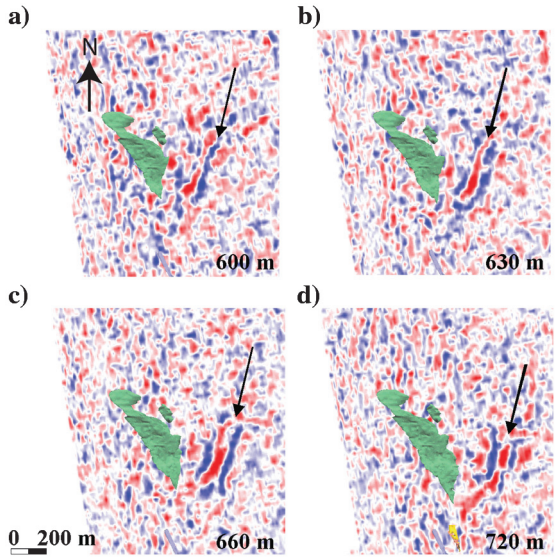

Figure 12. Horizontal slices from the DMO stack volume showing diffraction/reflection response (highlighted by arrows) from the same Callinan ore lens (green body) as shown in Figure 11.

Hostrock composition

The composition of the country rock that hosts the ore zones varies significantly and can have an appreciable effect on the ability to image the ore zones. This lithologic variability is demonstrated in Figure 17 where a detailed volumetric model for the camp (see Malinowski et al., 2012 for details) is compared directly with the corresponding observed seismic response. In the vicinity of the upper Callinan ore zone where a strong seismic response is observed in the field data (consistent with modeling results of Malinowski et al., 2012), there is very limited rhyolite within the mine horizon that surrounds the ore deposits. This provides strong evidence that the reflection response is directly associated with the ore/backfilled

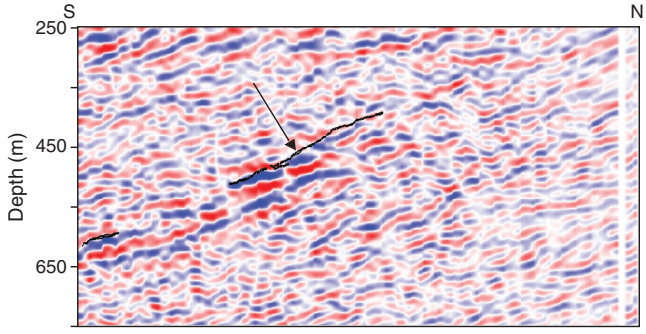

Figure 14. A plunge-section (orthogonal to Figure 13a) through the migrated seismic volume showing the phase reversal and the level (indicated by the arrow) across which a transition occurs from unmined ore above to backfill below. The black line outlines the ore zone intersections. Horizontal scale = vertical scale.

Figure 13. Dip sections from the migrated seismic volume and the corresponding Callinan ore lens intersections superposed. Subsequent sections progress from north-to-south showing the ore lens increasing in depth. Black lines indicate the ore lens intersections based on detailed mining and drillhole information. Horizontal scale = vertical scale.

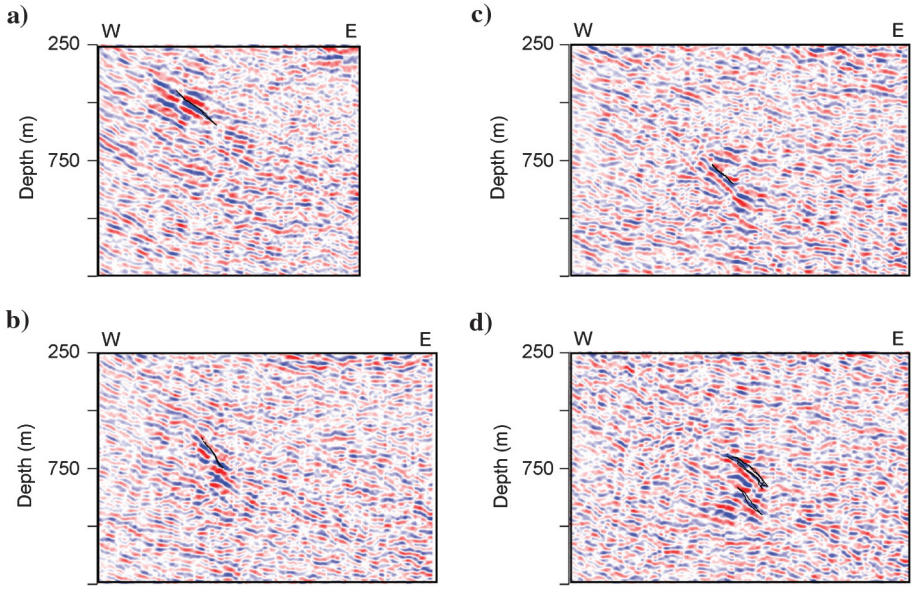

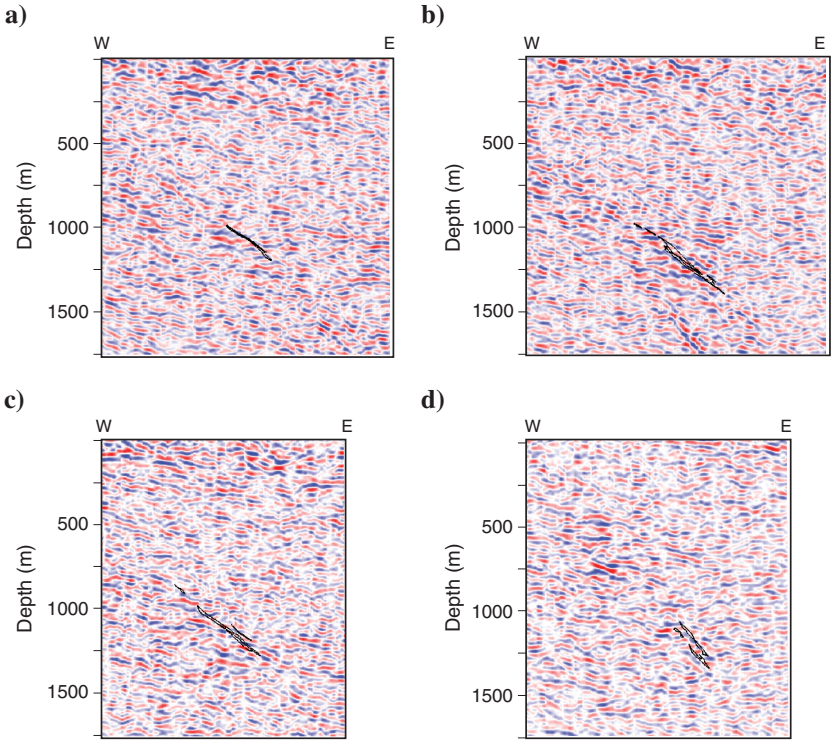

Figure 15. Vertical dip sections through the 777 ore lenses with subsequent sections ordered north to south showing lens increasing in depth. Seismic data are migrated. Black lines indicate the ore lens intersections based on detailed mining and drillhole information. Horizontal scale = vertical scale.

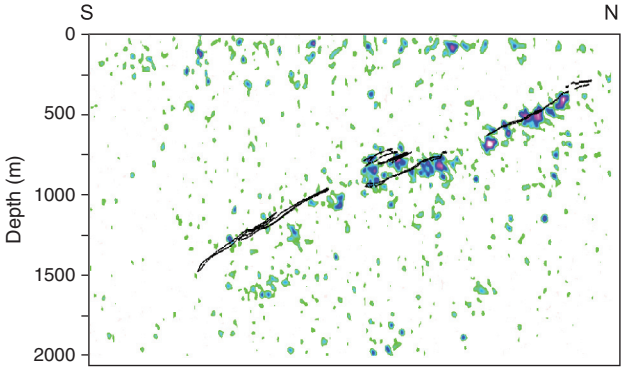

Figure 16. (a) Vertical slice through a 3D volume that constitutes the envelope amplitude attribute calculated for the migrated seismic data. This slice is closely located relative to the comparable vertical slice shown in Figure 10. Horizontal scale = vertical scale.

zones. In the vicinity of the deeper stacked Callinan ore zones, and even more so for the 777 deposits, the volume of rhyolite surrounding the ore zones increases. As shown by Malinowski et al. (2012), the result of the increasing presence of rhyolite is that the seismic response from the mine horizon becomes a more complex superposition of reflections/diffractions due to the strong scattering from the ore zones and hosting rhyolites within the background of basalts. Thus, although the mine horizon remains essentially reflective, the resultant images tend to be more highly variable. Furthermore, the recognition that the elastic properties of the mine horizon are simplified in this lithologic model (e.g., alteration effects can be significant, cautions against making overly elaborate interpretations from the seismic images.

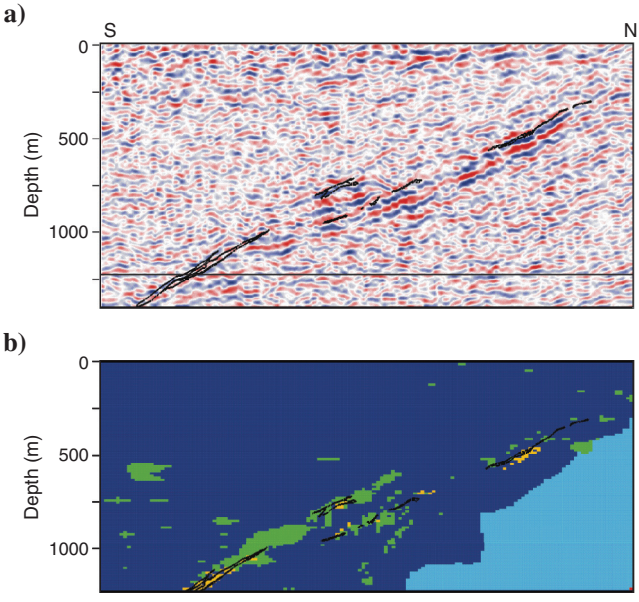

Figure 17. (a) Vertical slice through the 3D migrated volume. The black rectangle outlines the area covered by the model shown in (b). (b) Corresponding slice through the 3D lithological model based on detailed drillhole information and used for seismic modeling. Dark blue = basalt, light blue = sandstone, green = rhyolite, and orange = ore. See Malinowski et al. (2012) for further details concerning the modeling. The detailed geometry of the ore lenses is superposed (black lines) in (a and b). Horizontal scale = vertical scale.

CONCLUSIONS

A 17-km^2 3D-3C seismic survey within the active Flin Flon mining camp produced 3D images that trace the known orebodies

and mine horizon at depth. The acquisition program that utilized mixed dynamite and vibroseis sources with ~3400 3C single sensors proved to be effective in adapting to the variety of terrain and cultural impediments in the area. Adequate signal-to-noise levels were achieved in the final processed data, but were limited by the use of vibroseis energy sources operating at low peak force over much of the area, the appearance of sporadic noise bursts on a significant proportion of the data traces, and the generally noisy background environment. A conventional DMO processing sequence followed by poststack migration proved more effective than prestack time migration processing in producing images that correlated well with the geology as constrained by detailed drillhole information. The key steps in data processing proved to be trace editing, statics determination, and application of DMO. A constant velocity model proved to be satisfactory for application of NMO/DMO. In the case of the deeper ore zones that were characterized by low signal-to-noise levels, poststack migration was important in focusing weak ore-related reflections.

Comparison of the migrated 3D seismic images with the subsurface location of known ore lenses and the mine horizon generally shows a very good correlation. A well-defined diffraction response from one of the shallower Callinan ore bodies is observed in the unmigrated data, with a corresponding phase reversal in the vicinity of the transition from intact ore to backfilled ore zone. The cross-sectional geometry of backfilled ore zones compares well with strong reflection amplitudes to depths of ~1000 m. At greater depths, the 777 ore deposit has a weaker seismic signature likely due to a combination of effects including: Fresnel zone effects, residence in a lower signal-to-noise region of the survey, reduced reflectivity due to the pyrrhotite-rich nature of the ore, and complex scattering due to the increased presence of rhyolite within the mine horizon. The 3D data show the feasibility of detecting and accurately locating ore zones as small as a few million tons to depths of up to 1500 m.

ACKNOWLEDGMENTS

Hudson Bay Mining and Smelting Co. funded the acquisition and processing of the 3D seismic data and provided extensive drillhole information to the project. Brett Pearson and Jason Levers (HBMS) provided details of the ore deposits. The seismic data were acquired by Kinetex Inc. and processed by Sensor Geophysics. Barbara Dietiker drafted the figures. M. Malinowski was supported by the HOMING scholarship from the Foundation for Polish Science. The manuscript benefited from constructive reviews by A. Malehmir, Stefan Buske, Niklas Juhojuntti, Gilles Bellefleur, and an anonymous reviewer. This is Geological Survey of Canada contribution no. 20120118.

REFERENCES

Adam, E., G. Arnold, C. Beaudry, L. Matthews, B. Milkereit, G. Perron, and R. Pineault, 1997, Seismic exploration for VMS deposits, Matagami, Quebec, *in*, A. G. Gubins ed., Proceedings of Exploration 97: Fourth Decennial International Conference on Mineral Exploration, Paper, 87, 433–438.

Adam, E., G. Perron, G. Arnold, L. Matthews, and B. Milkereit, 2003, 3D seismic imaging for VMS deposit exploration, Matagami, Quebec *in* D. W. Eaton, B. Milkereit, and H. Salisbury, eds., Hardrock seismic exploration: SEG, Geophysical Development Series, 10, 229–246.

Adam, E., W. Qian, and B. Milkereit, 2007, In the shadow of a headframe: Deep exploration using integrated 3-D seismic and BHEM at the Louvicourt mine, Quebec, *in* B. Milkereit, ed., Proceedings of Exploration 07: 5th Decennial International Conference on Mineral Exploration, 1049–1053.

Eaton, D. W., E. Adam, B. Milkereit, M. Salisbury, B. Roberts, D. White, and J. Wright, 2010, Enhancing base-metal exploration with seismic imaging: Canadian Journal of Earth Sciences, **47**, 741–760, doi: 10.1139/E09-047.

Galley, A. G., E. C. Syme, and A. H. Bailes, 2007, Metallogeny of the Paleoproterozoic Flin Flon Belt, Manitoba and Sakatchewan, *in* W. D. Goodfellow, ed., Mineral deposits of Canada: A synthesis of major deposit types, district metallogeny, the evolution of geological provinces and exploration methods: Geological Association of Canada, Mineral Deposit Division, Special Publication no. 5, 509–531.

Gingerich, J. C., L. S. Matthews, and M. J. Pleshko, 2002, The development of new exploration technologies at Noranda: Seeing more with hyperspectral and deeper with 3D seismic: Canadian Institute of Mining Bulletin, **1058**, 56–61.

Hajnal, Z., and M. R. Stauffer, 1975, The application of seismic reflection techniques for subsurface mapping in the Precambrian shield near Flin Flon, Manitoba: Canadian Journal of Earth Sciences, 2036–2047, doi: 10.1139/e75-180.

Jones, P. R., 2001, The 777 Project — Creating a new future: Canadian Institute of Mining Bulletin, **1052**, 67–70.

Lucas, S. B., D. White, A. Hajnal, J. Lewry, A. Green, H. Zwanzig, K. Ashton, D. Schledewitz, A. Norman, P. Williams, R. Clowes, M. Stauffer, and G. Spence, 1994, Three-dimensional structure of the Trans-Hudson Orogen: Implications for collisional and post-collisional deformation history: Tectonophysics, **232**, 161–178, doi: 10.1016/0040-1951(94)90082-5.

Malehmir, A., and G. Bellefleur, 2009, 3D seismic reflection imaging of volcanic-hosted massive sulphide deposits: Insights from reprocessing Halfmile Lake data, New Brunswick, Canada: Geophysics, **74**, no. 6, B209–B219, doi: 10.1190/1.3230495.

Malinowski, M., E. Schetselaar, and D. J. White, 2012, 3D seismic imaging in the Flin Flon mining camp: Part 2 — Forward modeling: Geophysics, this issue.

Milkereit, B., E. K. Berrer, A. Watts, and B. Roberts, 1997, Development of 3-D seismic exploration technology for Ni-Cu deposits, Sudbury Basin, *in* A. G. Gubins ed., Proceedings of Exploration 97: 4th Decennial International Conference on Mineral Exploration, Paper 87, 439–448.

Milkereit, B., D. J. White, and A. G. Green, 1994, Towards an improved seismic imaging technique for crustal structures: The LITHOPROBE Sudbury experiment: Geophysical Research Letters, **21**, 927–930, doi: 10.1029/93GL02689.

Pretorius, C. C., W. F. Trewick, and C. Irons, 1997, Application of 3-D seismics to mine planning at Vaal Reefs Gold Mine, Number 10 shaft, Republic of South Africa, *in* A. G. Gubins, ed., Proceedings of Exploration 97: 4th Decennial International Conference on Mineral Exploration, Paper 87, 399–408.

Roberts, B., E. Zaleski, G. Perron, E. Adam, L. Petrie, and M. Salisbury, 2003, Seismic exploration of the Manitouwadge Greenstone Belt, Ontario: A case history, *in* D. W. Eaton, B. Milkereit, and H. Salisbury, eds., Hardrock seismic exploration: SEG, Geophysical Development Series, 10, 110–126.

Sheriff, R. E., and L. P. Geldart, 1984, Exploration Seismology, 2nd ed., Cambridge University Press.

Syme, E. C., and A. H. Bailes, 1993, Stratigraphic and tectonic setting of early Proterozoic volcanogenic massive sulphide deposits, Flin Flon, Manitoba: Economic Geology, **88**, 566–589, doi: 10.2113/gsecongeo.88.3.566.

White, D. J., S. B. Lucas, Z. Hajnal, A. G. Green, J. F. Lewry, W. Weber, H. V. Zwanzig, A. H. Bailes, E. C. Syme, J. Macek, K. E. Ashton, and D. J. Thomas, 1994, Early Proterozoic thick-skinned tectonics: LITHOPROBE seismic reflection results from the eastern Trans-Hudson Orogen: Canadian Journal of Earth Sciences, **31**, 458–469, doi: 10.1139/e94-042.

White, D. J., J. Mwenifumbo, and M. H. Salisbury, 2012b, Seismic properties of rocks from the Flin Flon Camp: (under minor revision for) Economic Geology, Flin Flon Special Issue.